Supplementary Appendix

This appendix has been provided by the authors to give readers additional information about their work.

Supplement to: Forde PM, Chaft JE, Smith KN, et al. Neoadjuvant PD-1 blockade in resectable lung cancer. N Engl J Med 2018;378:1976-86. DOI: 10.1056/NEJMoa1716078

Neoadjuvant PD-1 Blockade in Resectable Lung Cancer

Patrick M. Forde, Jamie E. Chaft, Kellie N. Smith, Valsamo Anagnostou, Tricia R. Cottrell, Matthew D. Hellmann, Marianna Zahurak, Stephen C. Yang, David R. Jones, Stephen Broderick, Richard J. Battafarano, Moises J. Velez, Natasha Rekhtman, Zachary Olah, Jarushka Naidoo, Kristen A. Marrone, Franco Verde, Haidan Guo, Jiajia Zhang, Justina X. Caushi, Hok Yee Chan, John-William Sidhom, Robert B. Scharpf, James White, Edward Gabrielson, Hao Wang, Gary L. Rosner, Valerie Rusch, Jedd D. Wolchok, Taha Merghoub, Janis M. Taube, Victor E. Velculescu, Suzanne L. Topalian, Julie R. Brahmer, Drew M. Pardoll

Supplementary Appendix

SUPPLEMENTARY METHODS 2
Pathology 2
Genomics/Neoantigens 3
Immunologic analyses 5
SUPPLEMENTARY FIGURES 8
Supplementary Figure S1: Study design and correlative analyses 8
Supplementary Figure S2: Recurrence-free survival 9
Supplementary Figure S3: Mutation signatures in major pathologic responders and non-responders 10
Supplementary Figure S4: Predicted mutation-associated neoantigen load is associated with response to anti-PD1. 11
Supplementary Figure S5: Clonal dynamics of circulating T cells 12
Supplementary Figure S6: Significant peripheral expansions of intra-tumoral T-cells. 13
Supplementary Figure S7: Multiplex immunoflourescence staining of the resected tumor bed from the subject featured in Figure 1A and B (patient 1) and Figure 4B-C 14
SUPPLEMENTARY TABLES 15
Table S1. Treatment-related adverse events 15
Table S2. Correlative assays performed by subject 16
Table S3: Pre-treatment clinical stage and post-treatment pathologic stage 17
Tables S4-S10: 18
SUPPLEMENTARY REFERENCES 18

SUPPLEMENTARY METHODS

Pathology

Immunohistochemical analysis

PD-L1 staining was performed on formalin-fixed, paraffin embedded (FFPE) tissue sections using the Dako PD-L1 IHC 28-8 pharmDx assay. Samples were considered to be PD-L1+ if ≥1% of tumor cells showed membranous PD-L1 expression. When multiple pre-treatment specimens were available for PD-L1 testing, the patient was considered PD-L1+ if any of the pre-treatment specimens were positive, and the highest percentage of PD-L1 positive tumor cells from all pre-treatment specimens is reported here.[1]

Selected specimens were assessed with multispectral immunofluorescence as previously described, with minor modifications.[2] Tumors were stained for simultaneous detection and quantitation of cytokeratin (tumor cells), CD8 (cytotoxic T cells), FoxP3 (regulatory T cells), CD68 (macrophages), PD-1, and PD-L1 as outlined in the table below. Multiplexed slides were scanned using the PerkinElmer Vectra3.0 (Perkin Elmer, Hopkington, MA) multispectral microscope and images were analyzed as previously described.[2]

Position	Antibody	Clone (host)/Company	Dilution	Incubation	TSA dyes
1	PD-L1	SP142 (rabbit)/Spring Bio.	1:1000	60 min	520
2	FoxP3	D608R (rabbit)/CST	1:800	30 min	570
3	PD-1	EPR4877(2) (rabbit)/AbCam	1:500	30 min	650
4	AE1/AE3	Mouse DAKO ref M3515	1:500	30 min	620
5	CD68	PGM-1(mouse)/Dako	1:400	30 min	690
6	CD8	4B11 (mouse)/AbD Ser	1:800	30 min	540
7	DAPI	Perkin Elmer Opal 7-color kit	2drops/ml	5 min	

Genomics/Neoantigens

Whole exome sequencing

Whole exome sequencing was performed on pre-treatment tumor and matched normal samples. Formalin fixed paraffin embedded (FFPE) tumor samples underwent pathological review for confirmation of lung cancer diagnosis and assessment of tumor purity. Tissue sections from each FFPE block were macrodissected to remove normal tissue. Matched normal samples were provided as peripheral blood. DNA was extracted from patients' tumors and matched peripheral blood using the Qiagen DNA FFPE and Qiagen DNA blood mini kit respectively (Qiagen, CA). Fragmented genomic DNA from tumor and normal samples was used for Illumina TruSeq library construction (Illumina, San Diego, CA) and exonic regions were captured in solution using the Agilent SureSelect v.4 kit (Agilent, Santa Clara, CA) according to the manufacturers' instructions as previously described.[3-5] Paired-end sequencing, resulting in 100 bases from each end of the fragments for the exome libraries was performed using Illumina HiSeq 2000/2500 instrumentation (Illumina, San Diego, CA). The mean depth of coverage for the tumor samples was 237x (**Supplementary Table S3**).

Primary processing of next-generation sequencing data and identification of putative somatic mutations

Somatic mutations were identified using the VariantDx custom software for identifying mutations in matched tumor and normal samples.[3] Prior to mutation calling, primary processing of sequence data for both tumor and normal samples was performed using Illumina CASAVA software (version 1.8), including masking of adapter sequences. Sequence reads were aligned against the human reference genome (version hg19) using ELAND with additional realignment of select regions using the Needleman-Wunsch method.[6] Candidate somatic mutations, consisting of point mutations, insertions, deletions as well as copy number changes were then identified using VariantDx across the whole exome. VariantDx examines sequence alignments of tumor samples against a matched normal while applying filters to exclude alignment and sequencing artifacts. In brief, an alignment filter was applied to exclude quality failed reads, unpaired reads, and poorly mapped reads in the tumor. A base quality filter was applied to limit

inclusion of bases with reported Phred quality score > 30 for the tumor and > 20 for the normal. A mutation in the pre- or post-treatment tumor samples was identified as a candidate somatic mutation only when (1) distinct paired reads contained the mutation in the tumor; (2) the fraction of distinct paired reads containing a particular mutation in the tumor was at least 10% of the total distinct read pairs; (3) the mismatched base was not present in >1% of the reads in the matched normal sample as well as not present in a custom database of common germline variants derived from dbSNP; and (4) the position was covered in both the tumor and normal. Mutations arising from misplaced genome alignments, including paralogous sequences, were identified and excluded by searching the reference genome. Candidate somatic mutations were further filtered based on gene annotation to identify those occurring in protein coding regions. Functional consequences were predicted using snpEff and a custom database of CCDS, RefSeq and Ensembl annotations using the latest transcript versions available on hg19 from UCSC.[7] Predictions were ordered to prefer transcripts with canonical start and stop codons and CCDS or RefSeq transcripts over Ensembl when available. Finally, mutations were filtered to exclude intronic and silent changes, while retaining mutations resulting in missense mutations, nonsense mutations, frameshifts, or splice site alterations. A manual visual inspection step was used to further remove artifactual changes.

Mutation signatures

We investigated differential mutational signatures from whole exome sequencing in patients achieving a MPR compared to those who did not.[8, 9] We extracted mutational signatures based on the fraction of mutations in each of 96 trinucleotide contexts and estimated the contribution of each signature to each tumor sample using the deconstructSigs R package.[9, 10]

Neoantigen predictions

To assess the immunogenicity of somatic mutations, exome data combined with each patient's MHC class I haplotype were applied in a neoantigen prediction platform that evaluates binding of somatic peptides to class I MHC, antigen processing, self-similarity and gene expression. Detected somatic mutations, consisting of nonsynonymous single base substitutions, insertions and deletions, were evaluated for putative neoantigens using the ImmunoSelect-R pipeline

(Personal Genome Diagnostics, Baltimore, MD). For single base substitutions, ImmunoSelect-R performs a comprehensive assessment of paired somatic and wild type peptides 8-11 amino acids in length at every position surrounding a somatic mutation. To accurately infer a patient's germline HLA 4-digit allele genotype, whole-exome-sequencing data from paired tumor/normal samples were first aligned to a reference allele set, which was then formulated as an integer linear programming optimization procedure to generate a final genotype by OptiType v1.0.[11] The HLA genotype served as input to netMHCpan to predict the MHC class I binding potential of each somatic and wild-type peptide (IC50 nM), with each peptide classified as a strong binder (SB), weak binder (WB) or non-binder (NB).[12-14] Peptides were further evaluated for antigen processing by netCTLpan and were classified as cytotoxic T lymphocyte epitopes (E) or non-epitopes (NA).[15] Paired somatic and wild-type peptides were assessed for self-similarity based on MHC class I binding affinity.[16] Neoantigen candidates meeting an IC50 affinity < 5000nM were subsequently ranked based on MHC binding and T-cell epitope classifications. Neoantigen candidates with an MHC affinity <500nM were further selected to estimate the neoantigen tumor burden and used in the statistical analyses. Tumor-associated expression levels derived from TCGA were used to generate a final ranking of candidate immunogenic peptides. Based on the netMHC pan algorithm applied to the neoantigens identified in each patent by WES, the top 47 predicted binders were synthesized and analyzed as described below.

Immunologic analyses

Stimulation and expansion of MANA-specific T cells

Functional assays were performed on T cells obtained from patient 01-005 prior to treatment (28 days prior to resection, D-28) and 44 days after resection (D+44). Forty seven mutation-associated neoantigen candidates (MANAs) were synthesized (Sigma-Aldrich, St. Louis, MO) and used in a novel T cell recognition assay, as previously described with minor modifications.[17, 18] Briefly, on day 0, T cells were isolated from D-28 and D+44 peripheral blood mononuclear cells (PBMCs) by negative selection (EasySep; STEMCELL Technologies). The T cell–negative fraction was gamma irradiated (3,000 rads) and co-cultured with an equal number of selected T cells in culture medium (AIM V with 50 μg/mL gentamicin) with 1 μg/mL relevant peptide, a CEF (CMV, EBV, and flu) peptide pool, or no peptide. On day 3, half the medium was replaced

with fresh medium containing cytokines for a final concentration of 50 IU/ml IL-2 (Chiron), 25 ng/ml IL-7 (Miltenyi), and 25 ng/ml IL-15 (PeproTech). On day 7, half the medium was replaced with fresh culture medium containing cytokines for a final concentration of 100 IU/mL IL-2 and 25 ng/mL IL-7 and IL-15. On day 10, cells were harvested, washed twice with PBS, and the $CD8^+$ fraction was isolated using a $CD4^+$ positive selection kit (EasySep; STEMCELL Technologies).

T cell receptor (TCR) sequencing

DNA was extracted from peptide-stimulated T cells, tumor tissue obtained prior to neoadjuvant nivolumab and at the time of surgical resection, and longitudinal pre- and post-treatment PBMCs using a Qiagen DNA FFPE kit, DNA blood kit, or DNA blood mini kit (Qiagen). TCR Vb CDR3 sequencing was performed using the survey (tissue and cultured cells) or deep (PBMC) resolution Immunoseq platforms (Adaptive Biotechnologies, Seattle, WA).[19] Bioinformatic and biostatistical analyses of productive clones were performed to assess the dynamics of peripheral T cells and to identify antigen-specific expansions. Peripheral T cell clones with >10 reads at the D-3 timepoint (3 days prior to surgery) were further analyzed for significant expansion. Antigen-specific T cell clones were identified in cultured peripheral T cells using the following criteria: 1) significant expansion of the relevant clone (Fisher exact test with Benjamini-Hochberg FDR, $p<0.001$) compared to T cells cultured without peptide, 2) significant expansion (Fisher exact test with Benjamini-Hochberg FDR, $p<0.001$) of this clone compared to every other peptide-stimulated culture, and 3) at least 10 reads in the relevant T cell culture. Expanded/antigen-specific clones that were also detected in the pre-treatment and/or resection tumor were further analyzed. In order to calculate the clonality of intratumoral T cells, the following equation was used:

$$Clonality = 1 - \frac{\sum_{i=1}^{S} p_i \ln(p_i)}{\ln(S)}$$

where S = total number of unique TCR sequences and p_i is the proportion of the repertoire made up by the *i*th sequence.

Statistics

Analysis of peripheral expansion of intratumoral clones was performed using Fisher's exact test with Benjamini-Hochberg correction for FDR. The association of pathological response with the intratumoral frequency of shared clones and the clonality of tumor infiltrating lymphocytes were assessed using the Wilcoxon signed-rank test. The differential enrichment in the C>A transversion-high signature in responders vs. non-responders was statistically evaluated using the Wilcoxon rank sum test.

SUPPLEMENTARY FIGURES

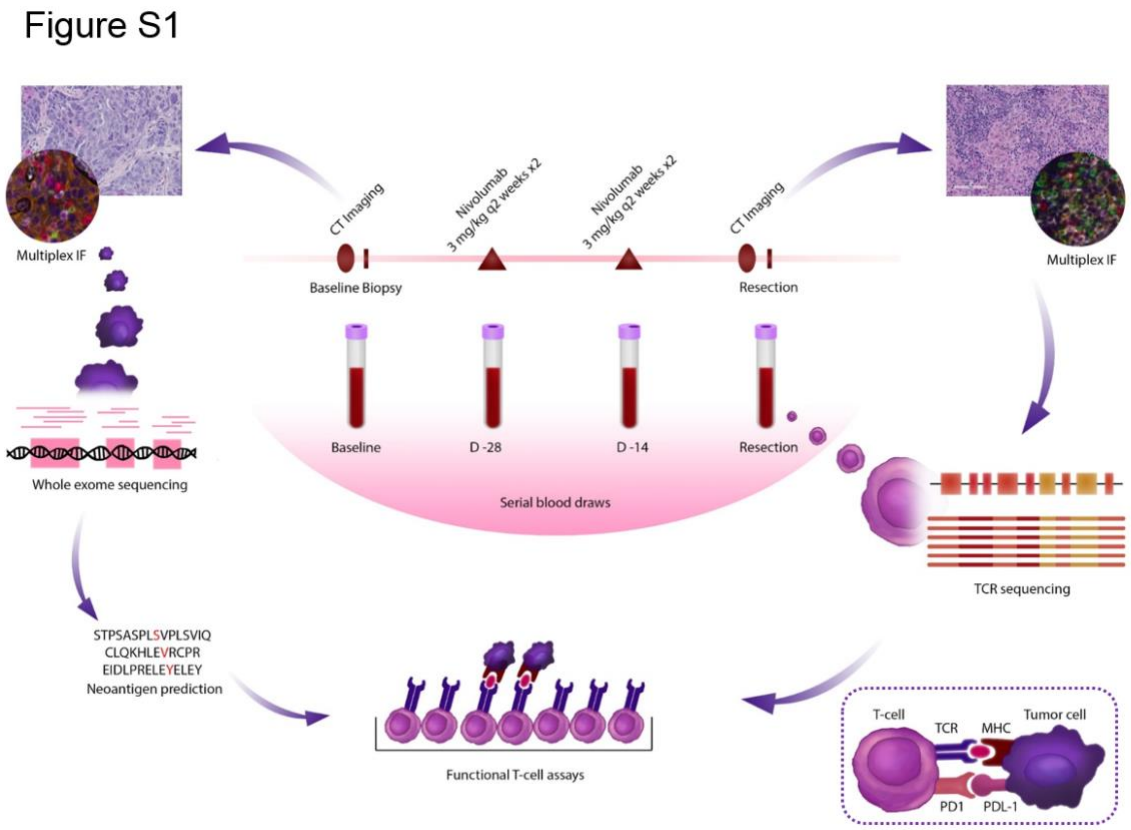

Supplementary Figure S1: Study design and correlative analyses

Nivolumab was administered at 3mg/kg every two weeks for 2 doses prior to surgical resection. Tumor samples were collected at baseline and at the time of resection alongside serial blood samples collected at baseline, day -28, day -14, time of resection and at the first postoperative clinic visit (weeks 3-8 after surgery). Multiplex immunofluorescence (IF) was performed on selected pre-treatment tumor and tumor resection specimens. In cases where sufficient tissues were available, assays were performed as follows. Whole exome sequencing was performed on matched pre-treatment tumor and normal samples. Exome data were applied in a neoantigen prediction pipeline that allows for generation of mutation-association neoantigen (MANA) candidates tailored to each patient's HLA haplotype. MANA-specific TCR (T-cell receptor) expansion was evaluated in stimulated autologous T-cell cultures. Dynamic changes in the TCR repertoire during anti-PD-1 therapy were assessed by TCR next-generation sequencing. Functional T-cell assays were performed in a case of primary tumor pathologic complete response (patient 1).

Figure S2

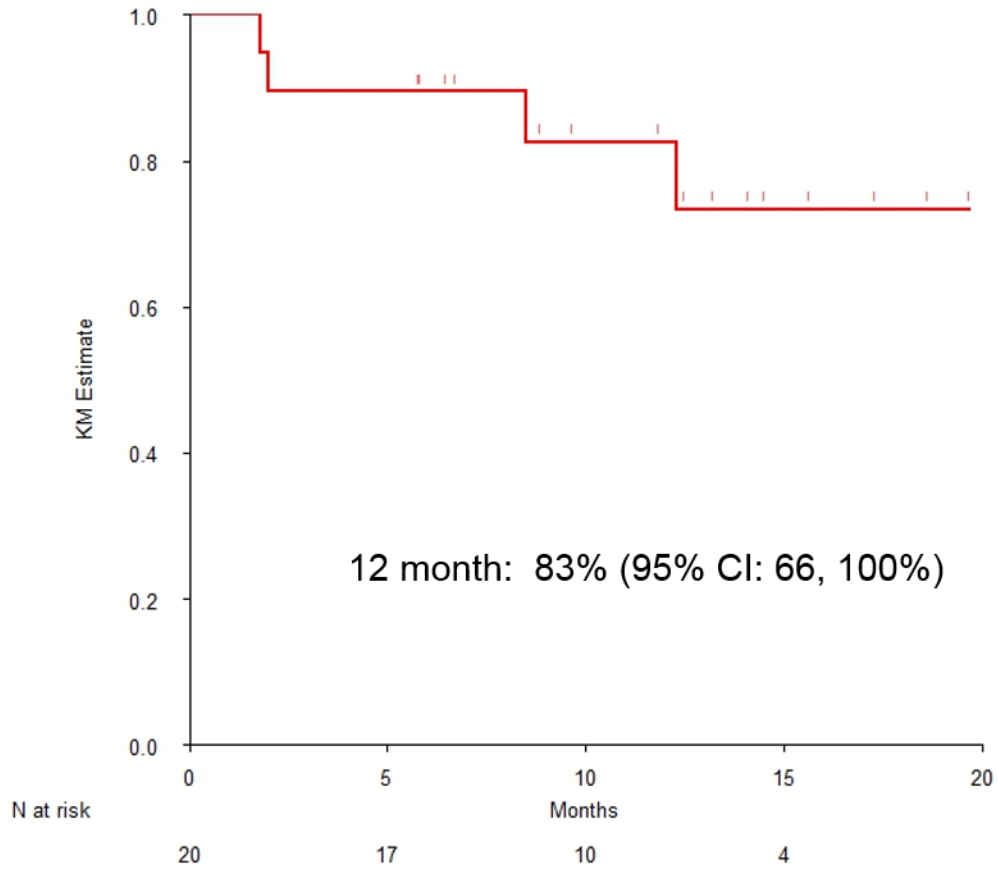

Supplementary Figure S2: Recurrence-free survival

Kaplan-Meier recurrence-free survival (RFS) estimates with 95% confidence intervals. RFS is calculated from the time of surgery to recurrence or death. With an overall median follow-up for the study of 12 months, the 12-month RFS is 83% (95% CI: 66, 100%). The numbers of patients at risk at 5-month intervals are included below the x-axis.

Figure S3

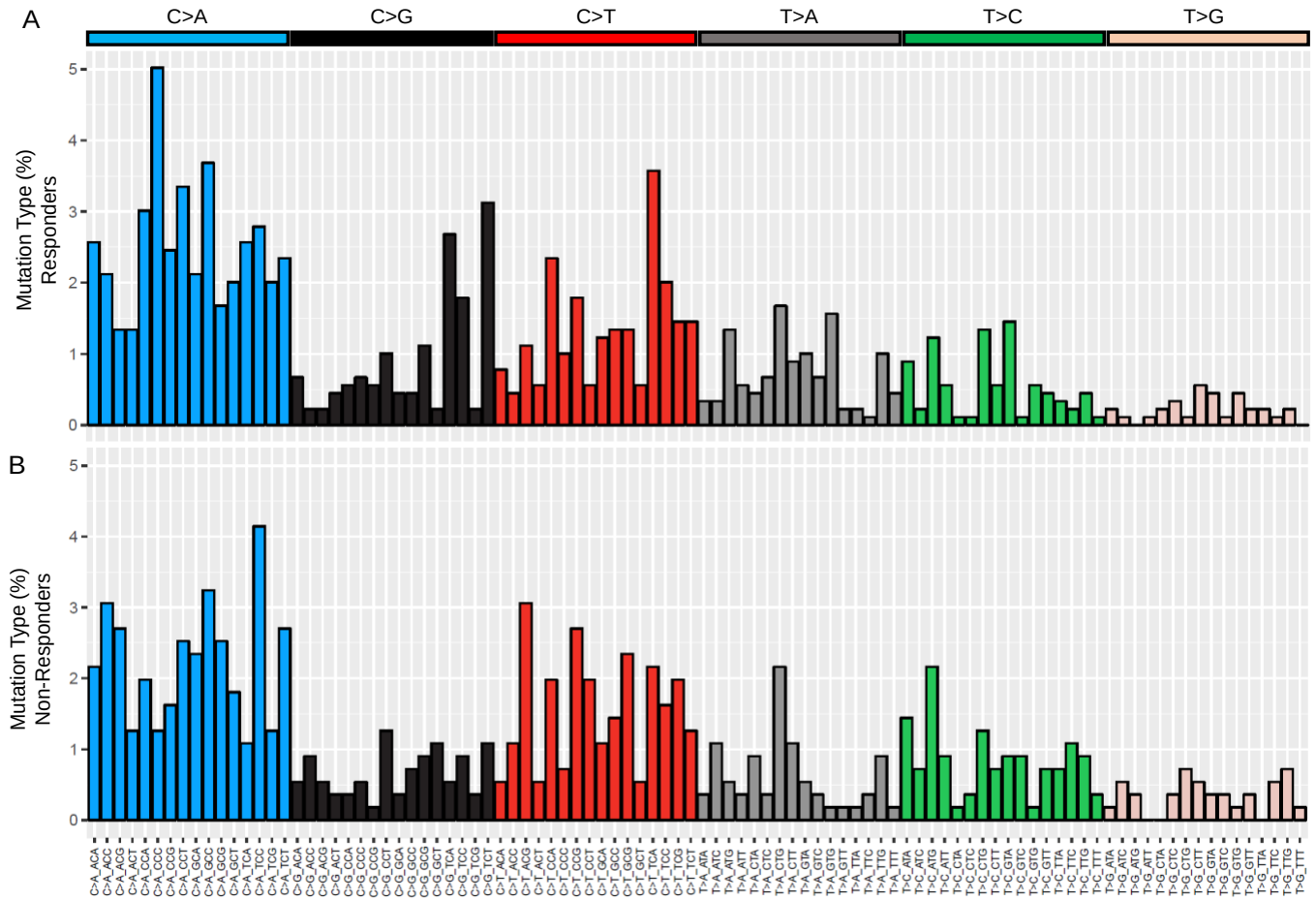

Supplementary Figure S3: Mutation signatures in major pathologic responders and non-responders

Mutational signatures are displayed based on six types of substitutions (C>A, C>G, C>T, T>A, T>C and T>G) and their sequence context in the 11 tumors analyzed (major pathologic responders, panel A; non-major-pathologic responders, panel B).[20] The mutation signatures were generated by incorporating the class of substitution as well as the bases immediately 5' and 3' to the mutated base. A slightly more prominent transversion-high signature (enriched in C>A single base substitutions, blue bars) was seen in responders compared to non-responders, however the differential enrichment did not reach statistical significance. Each mutational signature is displayed using a 96 substitution classification defined by the substitution class and the sequence context immediately 3' and 5' to the mutated base. The mutation types are shown on the horizontal axes and the vertical axes depict the percentage of mutations attributed to a specific mutation type (blue: C>A, black: C>G, red: C>T, gray: T>A, green: T>C, beige: T>G).

Figure S4

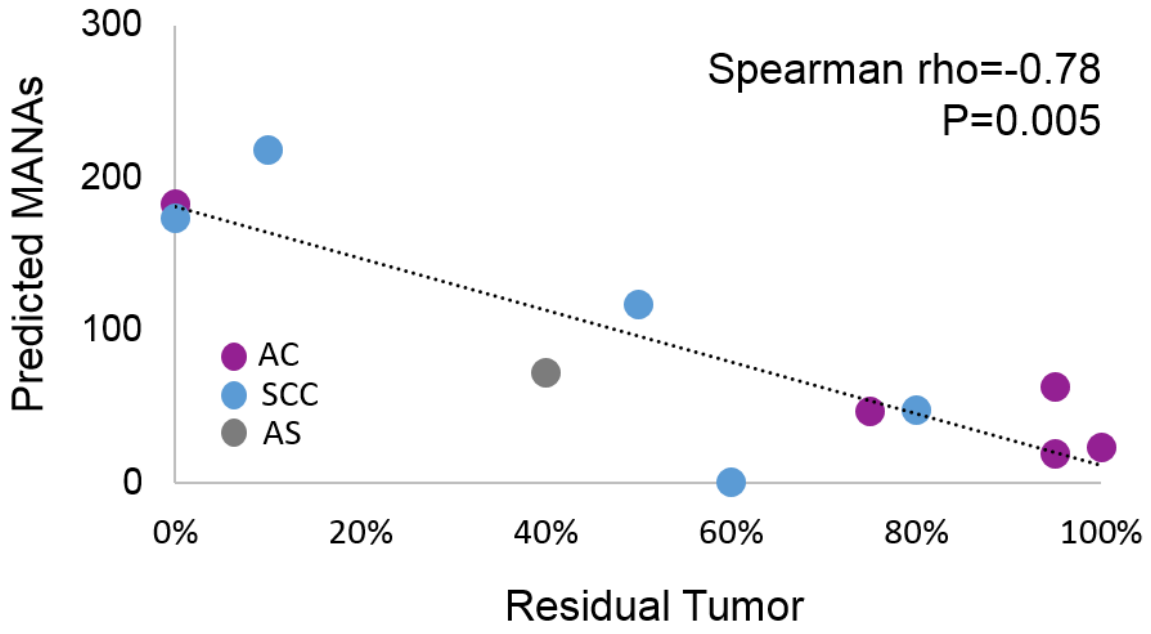

Supplementary Figure S4: Predicted mutation-associated neoantigen load is associated with response to anti-PD1.

Neoantigen candidates with a predicted MHC affinity <500 nM were selected to estimate the neoantigen burden per tumor; the number of candidate neoantigens was found to be inversely associated with the percent residual tumor after nivolumab treatment (Spearman R= -0.78, p=0.005). Blue circles, squamous non-small-cell lung cancer; purple circles, non-squamous non-small-cell lung cancer; gray circle, adenosquamous non-small-cell lung cancer.

Figure S5

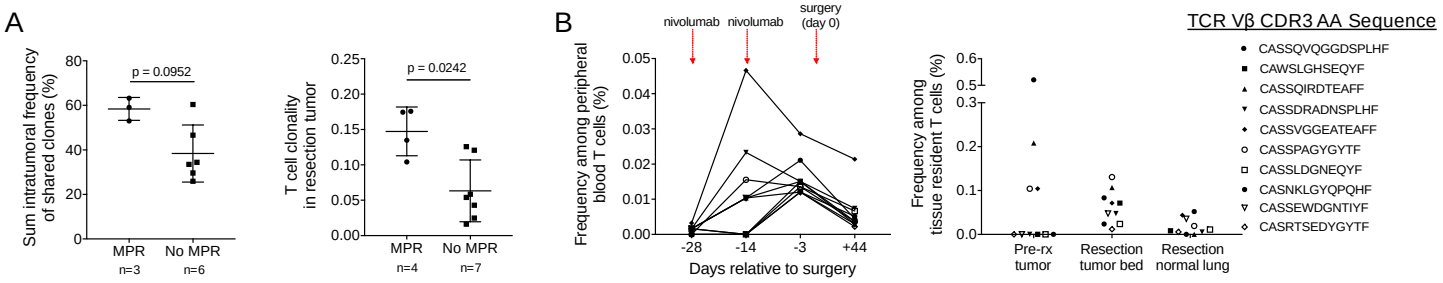

Supplementary Figure S5: Clonal dynamics of circulating T cells

(**A**) **Left panel:** In 9 patients with matched pre-treatment and post-operative blood samples, T-cell receptor (TCR) Vβ CDR3 sequencing was performed on pre-treatment and peri-operative peripheral T-cells, pre-treatment tumor biopsies, and post-treatment tumor derived from the surgical resection. The sum of intra-tumoral frequencies of shared clones, defined as clones that were found in both the tumor and periphery at the time of resection, is shown for patients with and without a MPR.

Right panel: The clonality of tumor infiltrating lymphocytes at the time of resection was analyzed for 11 resected tumors with and without a MPR. Since this analysis did not involve matched blood samples, two additional patients' tumor-infiltrating lymphocytes, for which matching peri-operative blood samples were not available, are included.

(**B**) T-cell receptor (TCR) Vβ CDR3 sequencing was performed on resected tumor, normal lung and peripheral blood of patient 1 to identify shared T-cell clones between tumor and peripheral blood. The frequency of shared intra-tumoral clones expanding in peripheral blood between treatment initiation and surgical resection at various time points is shown (left panel). Representation of these clones was lower in normal lung from the resection specimen (right panel).

Figure S6

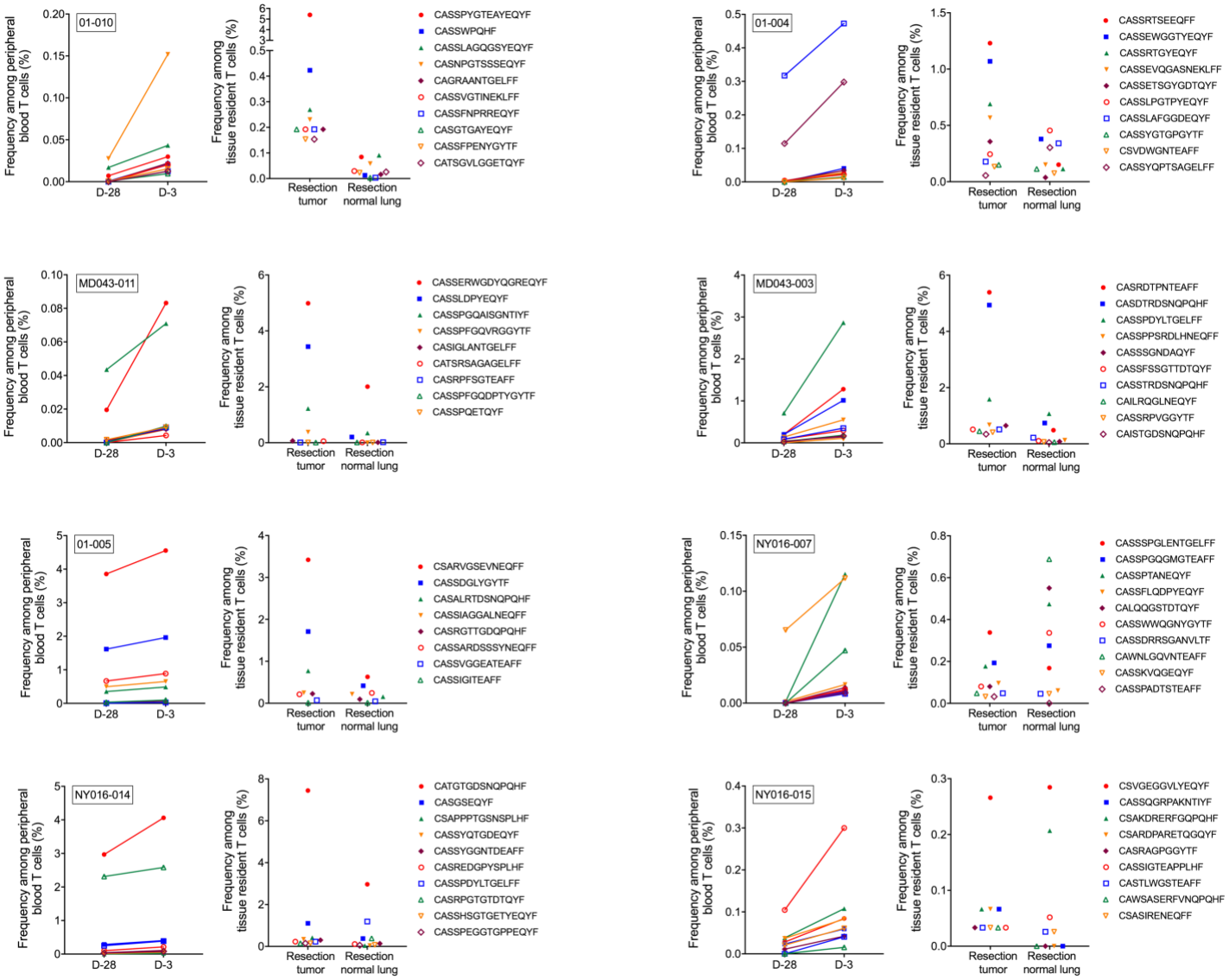

Supplementary Figure S6: Significant peripheral expansions of intra-tumoral T-cells.
In 9 patients (3 MPR, 6 non-MPR), T-cell receptor (TCR) Vβ CDR3 sequencing was performed on pre-treatment (D-28) and pre-operative (D-3) peripheral blood as well as tumor and normal lung tissue specimens obtained at the time of resection. Figures show the 10 most frequent intra-tumoral clones in each of 8 patients in whom these clones also underwent significant expansions in the periphery. Data are displayed as the percentage of dominant clonal TCRs among all TCR reads detected.

Figure S7

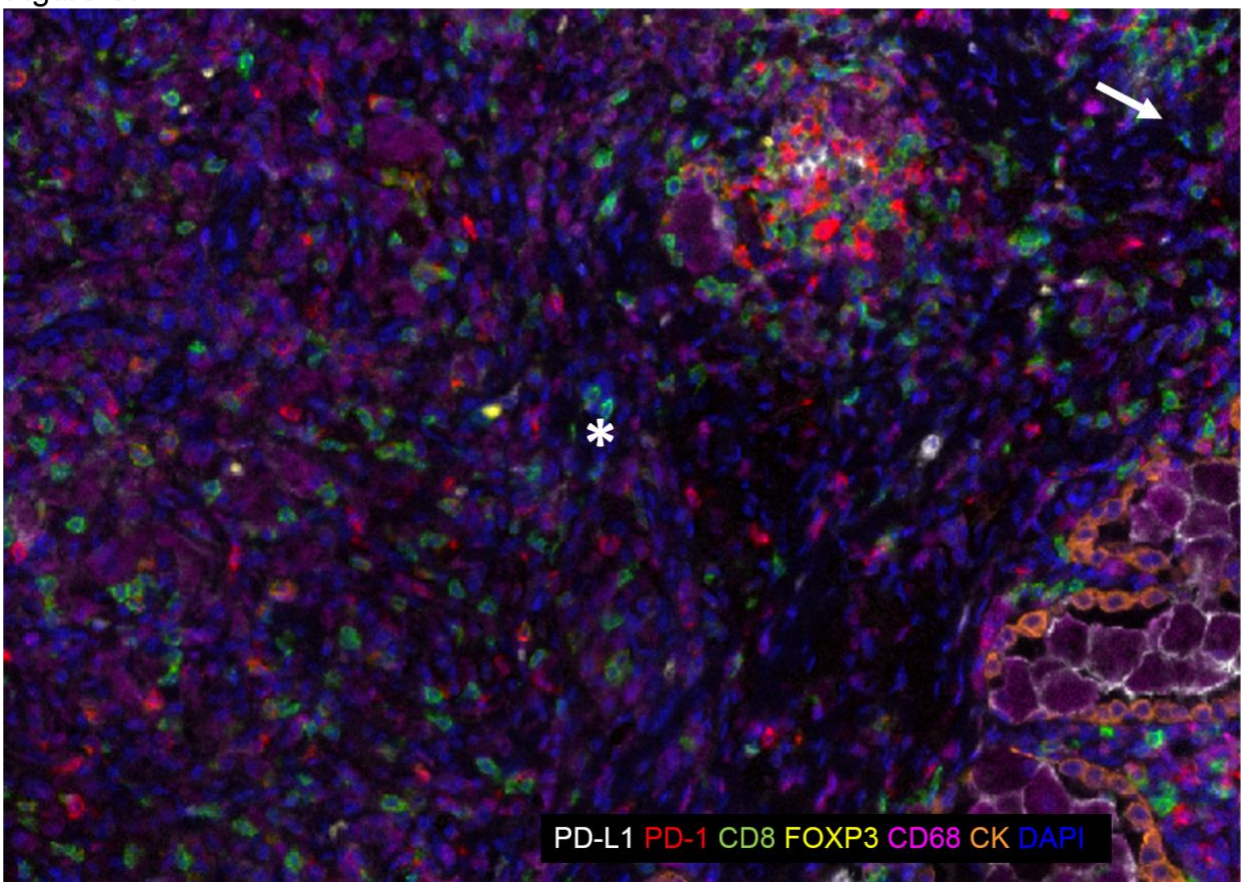

Supplementary Figure S7: Multiplex immunoflourescence staining of the resected tumor bed from the subject featured in Figure 1A and B (patient 1) and Figure 4B-C

There was a complete pathologic response in the 8cm primary tumor.
The tumor bed (asterisk) is infiltrated by abundant CD8+ T-cells (green), PD-1+ lymphocytes (red), and CD68+ macrophages (magenta), including the formation of a tertiary lymphoid structure (arrow). Rare FoxP3+ T regulatory cells are present (yellow). Adjacent alveoli (arrowhead) are lined by non-neoplastic epithelial cells expressing cytokeratin (orange) and filled with CD68+ macrophages expressing PD-L1 (white). 200x original magnification. Microscopic tumor deposits were found in 4 lymph nodes (not shown).

SUPPLEMENTARY TABLES

Table S1. Treatment-related adverse events

N=22 (All patients who received at least 1 dose of nivolumab)	Grade 1-2 n (%)	Grade 3-4 n (%)
Fever	1 (5)	0
GI: Abdominal pain Anorexia/dysgeusia Vomiting/diarrhea LFT abnormality	 1 (5) 3 (14) 2 (10) 1 (5)	 0 0 0 0
Infusion reaction	1 (5)	0
Dry Skin	1 (5)	0
CNS (delirium)	1 (5)	0
Pneumonia	0	1 (5)

Table S2. Correlative assays performed by subject

(X= assay performed; NA=assay not performed)

Patient number	Study ID number	Genomics identifier	PD-L1 IHC	Exome sequencing	Peripheral blood TCRseq	Tumor TCRseq
1	MD01-005	CGLU204	NA	X	X	X
2	MD043-003	CGLU206	NA	NA	X	X
3	MD01-004	CGLU205	X	X	X	X
4	MD043-008	CGLU215	X	X	NA	X
5	MD01-010	CGLU223	X	NA	X	X
6	MD043-012	CGLU217	X	X	NA	NA
7	MD043-011	CGLU222	X	X	X	X
8	MD01-019	CGLU224	X	X	NA	X
9	MD043-006	CGLU221	X	X	NA	X
10	MD043-023	CGLU265	NA	NA	NA	NA
11	MD01-024	CGLU264	X	X	NA	NA
12	NY016-007	CGLU218	X	X	X	X
13	NY016-009	CGLU219	X	NA	X	X
14	NY016-014	CGLU220	X	X	X	X
15	NY016-015	CGLU225	NA	NA	X	X
16	NY016-016	CGLU259	X	X	NA	NA
17	NY016-017	CGLU290	NA	X	NA	NA
18	NY016-020	CGLU249	NA	NA	NA	NA
19	NY016-021	CGLU279	X	NA	NA	NA
20	NY016-022	CGLU250	X	NA	NA	NA
21	NY016-025	CGLU256	X	NA	NA	NA

Table S3: Pre-treatment clinical stage and post-treatment pathologic stage

Patient number	Pre-treatment clinical stage TNM (stage group)	Pathologic stage at resection TNM (stage group)	Major Pathologic Response (yes/no)	Pathologic downstaging (yes/no)
1	T3N0* (IIB)	T0N1* (IIA)	Yes	Yes
2	T2AN0 (IB)	T2AN0 (IB)	Yes	No
3	T4N1 (IIIA)	T4N1 (IIIA)	No	No
4	T1BN0 (IA)	T1BN0 (IA)	Yes	No
5	T3N0 (IIB)	T2BN0 (IIA)	Yes	Yes
6	T3N1 (IIIA)	T3N1 (IIIA)	No	No
7	T2AN1 (IIA)	T3N1 (IIIA)	No	No
8	T2AN0 (IB)	T2AN0 (IB)	No	No
9	T2AN1 (IIA)	T1AN1 (IIA)	No	No
10	T1AN2 (IIIA)	T1AN0 (IA)	Yes	Yes
11	T1AN0 (IA)	T2AN0 (IB)	No	No
12	T2AN1 (IIA)	T2AN0 (IB)	No	Yes
13	T1AN2 (IIIA)	T2AN2 (IIIA)	No	No
14	T2N2 (IIIA)	T2N2M1a (IV)**	No	No
15	T2BN1 (IIA)	T3N1 (IIIA)	No	No
16	T1BN1 (IIA)	T0N0	Yes	Yes
17	T2AN2 (IIIA)	Unresectable	No	No
18	T2BN1 (IIB)	T1BN0 (IB)	Yes	Yes
19	T3N0 (IIB)	T3N1 (IIIA)	No	No
20	T2bN0 (IIA)	T1AN0 (IA)	Yes	Yes
21	T3N1 (IIIA)	T0N0	Yes	Yes

*Nodal stations 7, 12R and 11R were biopsied pre-treatment via EBUS and were negative. Pre-treatment PET/CT showed uptake in the 8cm primary tumor which was contiguous with the hilum. Post-treatment the N1 nodal station 10R was positive for residual tumor cells, the primary tumor underwent complete pathologic response.

**Stage IV by virtue of resected pleural implant. No further systemic therapy and patient remains without evidence of disease progression.

Tables S4-S10: See included Excel file.

SUPPLEMENTARY REFERENCES

1. Taube JM, Klein A, Brahmer JR, et al. Association of PD-1, PD-1 ligands, and other features of the tumor immune microenvironment with response to anti-PD-1 therapy. Clin Cancer Res 2014;20:5064-74.
2. Nghiem PT, Bhatia S, Lipson EJ, et al. PD-1 Blockade with pembrolizumab in advanced Merkel-cell carcinoma. N Engl J Med 2016;374:2542-52.
3. Sausen M, Leary RJ, Jones S, et al. Integrated genomic analyses identify ARID1A and ARID1B alterations in the childhood cancer neuroblastoma. Nature Genet 2013;45:12-7.
4. Jones S, Anagnostou V, Lytle K, et al. Personalized genomic analyses for cancer mutation discovery and interpretation. Sci Transl Med 2015;7:283ra53.
5. Bertotti A, Papp E, Jones, et al. The genomic landscape of response to EGFR blockade in colorectal cancer. Nature 2015;526:263-7.
6. Needleman SB, Wunsch CD. A general method applicable to the search for similarities in the amino acid sequence of two proteins. J Mol Biol 1970;48:443-53
7. UCSC. https://genome.ucsc.edu/.
8. Sjöblom T, Jones S, Wood LD, et al. The consensus coding sequences of human breast and colorectal cancers. Science 2006;314:268-74.
9. Alexandrov LB, Nik-Zainal S, Wedge DC, et al. Signatures of mutational processes in human cancer. Nature 2013;500:415-21.
10. https://CRAN.R-project.org/package=deconstructSigs
11. Szolek A, Schubert B, Mohr C, Sturm M, Feldhahn M, Kohlbacher O, et al. OptiType: precision HLA typing from next-generation sequencing data. Bioinformatics 2014;30:3310-6.

12. Nielsen M, Andreatta M. NetMHCpan-3.0; improved prediction of binding to MHC class I molecules integrating information from multiple receptor and peptide length datasets. Genome Med 2016;8:33.
13. Lundegaard C, Lamberth K, Harndahl M, Buus S, Lund O, Nielsen M. NetMHC-3.0: accurate web accessible predictions of human, mouse and monkey MHC class I affinities for peptides of length 8-11. Nucleic Acids Res 2008;36:W509-12
14. Lundegaard C, Lund O, Nielsen M. Accurate approximation method for prediction of class I MHC affinities for peptides of length 8, 10 and 11 using prediction tools trained on 9mers. Bioinformatics 2008 Jun 1;24(11):1397-8.
15. Stranzl T, Larsen MV, Lundegaard C, Nielsen M. NetCTLpan: pan-specific MHC class I pathway epitope predictions. Immunogenetics 2010;62:357-68.
16. Kim Y, Sidney J, Pinilla C, Sette A, Peters B. Derivation of an amino acid similarity matrix for peptide: MHC binding and its application as a Bayesian prior. BMC Bioinformatics 2009;10:394.
17. Anagnostou V, Smith KN, Forde PM, et al. Evolution of neoantigen landscape during immune checkpoint blockade in non-small cell lung cancer. Cancer Discov 2017;7:264-276.
18. Le DT, Durham JN, Smith KN, et al. Mismatch repair deficiency predicts response of solid tumors to PD-1 blockade. Science 2017;357:409-413.
19. Srivastava SK, Robins HS. Palindromic nucleotide analysis in human T cell receptor rearrangements. PLoS One. 2012;7(12):e52250.
20. Alexandrov LB, Nik-Zainal S, Wedge DC, et al. Signatures of mutational processes in human cancer. Nature 2013;500:415-21.